Synthesis, characterization, and CO_2 uptake of mellitic triimide-based covalent organic frameworks

Veldhuizen, Hugo; Vasileiadis, Alexandros; Wagemaker, Marnix; Mahon, Tadhg; Mainali, Durga P.; Zong, Lishuai; van der Zwaag, Sybrand; Nagai, Atsushi

DOI
10.1002/pola.29510

Publication date
2019

Document Version
Final published version

Published in
Journal of Polymer Science, Part A: Polymer Chemistry

Synthesis, Characterization, and CO_2 Uptake of Mellitic Triimide-Based Covalent Organic Frameworks

Hugo Veldhuizen,[1] **Alexandros Vasileiadis**,[2] **Marnix Wagemaker**,[2] **Tadhg Mahon**,[1] **Durga P. Mainali**,[3] **Lishuai Zong**,[1] **Sybrand van der Zwaag**,[1] **Atsushi Nagai**[1]

[1]Novel Aerospace Materials group, Delft University of Technology, Kluyverweg 1, 2629 HS Delft, The Netherlands
[2]Storage of Electrochemical Energy group, Delft University of Technology, Mekelweg 15, 2629 JB Delft, The Netherlands
[3]Delft Aerospace Structures and Materials Laboratory, Delft University of Technology, Kluyverweg 3, 2629 HS Delft, The Netherlands
Correspondence to: A. Nagai (E-mail: a.nagai@tudelft.nl)

Received 23 July 2019; Revised 9 September 2019; accepted 16 September 2019
DOI: 10.1002/pola.29510

KEYWORDS: A_3–B_3 monomers; CO_2 uptake; covalent organic framework; imidization; mellitic triimide; porous polymers; polyimides; polycondensation; microporous materials

Among the material class of organic porous polymers, covalent organic frameworks (COFs) are a special subclass, because of their crystalline nature.[1] Moreover, depending on the building blocks, COFs can be designed with predictable pore shapes and sizes. The uniform and controlled porosity as a result of their crystallinity makes COFs perfect candidates for separation of gasses,[2] as well as purification of liquids.[3] Furthermore, redox-active COFs with a high surface area have become an increasingly interesting class of material for electrochemical energy storage devices.[4,5] Whatever the application, a high thermal and chemical stability of the structural linkages of COFs is very important and this drove the direction of the research as reported in this paper.

Generally, dynamic covalent chemistry is a requisite for the creation of crystalline COFs, since it allows for error checking and reparation of amorphous segments in order to form the thermodynamically stable structure (i.e., the crystal). For this reason, highly reversible boroxine and boronate ester bonds where the first to be employed as connecting linkages in COFs.[6,7] Although these early COFs were not excellent in terms of stability, recent advances were made toward the development of structurally more robust frameworks.[8–11] In particular, polyimide COFs bring a high chemical and thermal stability to this material class,[8,12,13] which will push their applicability forward.

In this research, we designed and synthesized mellitic triimide (MTI)-based COFs derived from mellitic trianhydride (MTA) with 1,3,5-tris(4-aminophenyl)benzene (TAPB) or 1,3,5-tris (4-aminophenyl)amine (TAPA) to yield **MTI-COF-1 or MTI-COF-2**, respectively. The combination of the small monomer MTA in the polymerization of A_3 with B_3 monomers contributes to the formation of porous (quasi-) crystalline materials with hexagonal micropores (<2 nm). In addition, MTI-based materials are being studied because of their excellent redox activity.[14–16] By utilizing MTI in an A_3–B_3 COF, we introduce a large number of active sites with respect to the overall molecular weight of the unit cell. Therefore, we envisage that this material could be interesting in both gas separation (due to its micropores) and energy storage (due to its redox-active groups) applications.

The synthesis of **MTI-COF-1** and **MTI-COF-2** goes via a polycondensation reaction of MTA as trianhydride with TAPB or TAPA as primary triamines respectively, using solvothermal conditions (Scheme 1). MTA was synthesized from mellitic acid and acetic anhydride (Supporting Information), while TAPB and TAPA were commercially obtained. The monomers were suspended in a mixed solvent of equal amounts of *meta*-cresol and *N*-methyl-2-pyrrolidone, and isoquinoline was used as the catalyst. Degassed reaction mixtures were flame sealed in glass ampules and left for 3 days in an oven at 150 °C. The resulting polymers were assessed regarding their chemical structure, crystallinity, and porosity.

Imide formation was confirmed with Fourier transform infrared (FTIR) spectroscopy [Fig. 1(A,B)]. For both COFs, the characteristic C⎕O anhydride peaks at 1791 (symm.) and 1871 (asymm.) cm^{-1} disappeared. Additionally, the N—H amine peaks around 3400 cm^{-1} for TAPB and TAPA were not detected in the obtained COF materials. Characteristic imide

Additional supporting information may be found in the online version of this article.

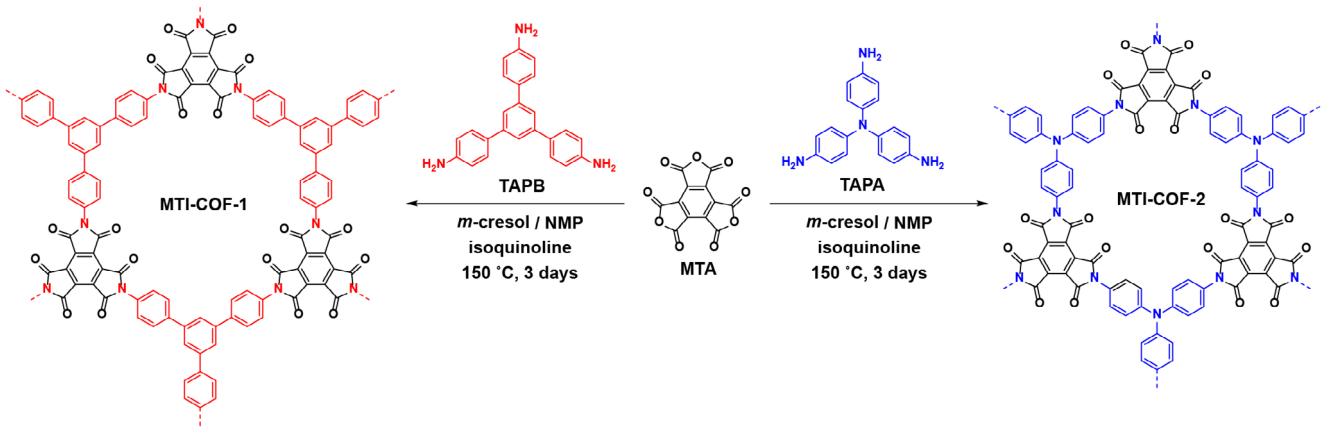

SCHEME 1 Polycondensation of MTA with TAPB, or TAPA to yield **MTI-COF-1**, or **MTI-COF-2**, respectively. [Color figure can be viewed at wileyonlinelibrary.com]

carbonyl (C⍰O) peaks around 1730 (symm.) and around 1780 cm^{-1} (assym.) were observed for both COF materials. Moreover, the broad peaks at 1372 and 1382 cm^{-1} for **MTI-COF-1** and **MTI-COF-2**, respectively, were attributed to imide C—N stretching. Thus, polyimide formation was confirmed for both COFs. Furthermore, the thermal properties of the polymers were determined by thermogravimetric analysis. The 5% weight loss decomposition temperatures for **MTI-COF-1** and **MTI-COF-2** were 291 and 275 °C, respectively (Supporting Information). Although still moderately thermally stable, these

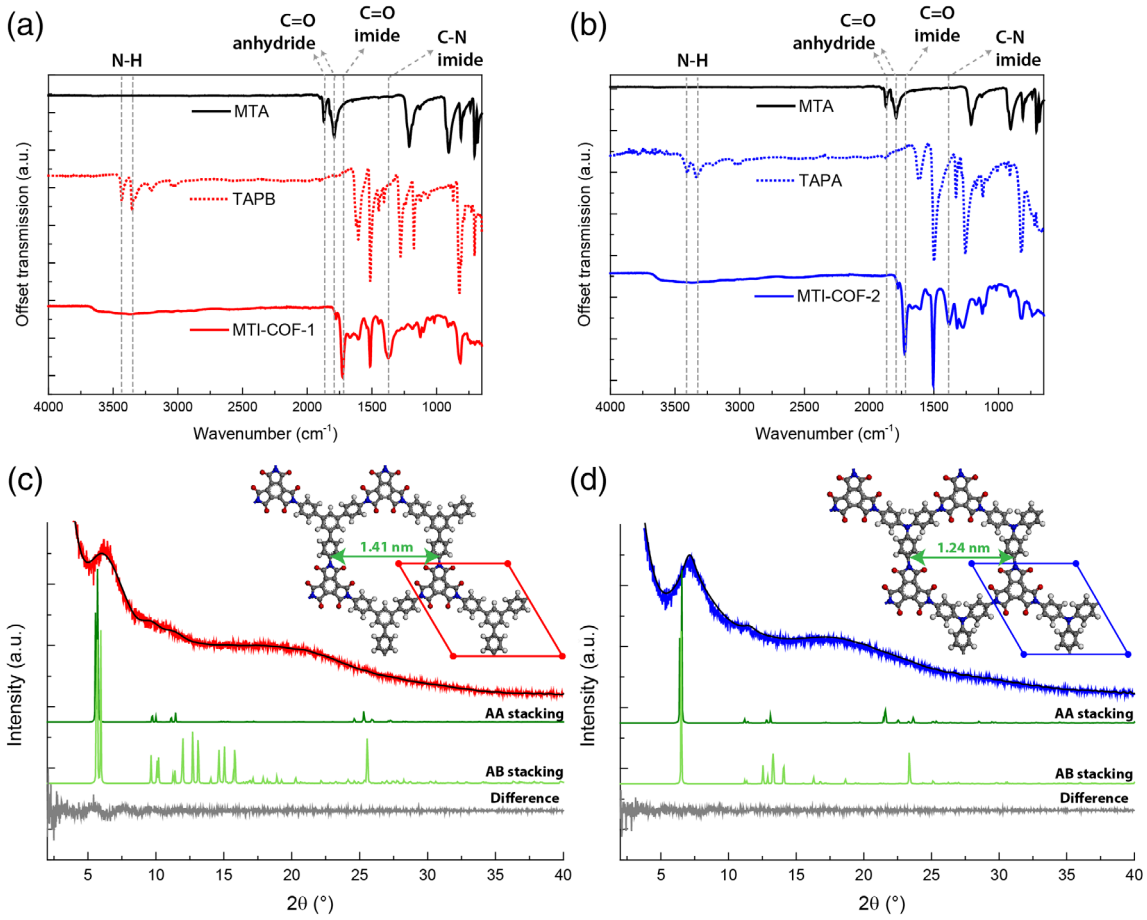

FIGURE 1 (A) FTIR spectra of monomers MTA and TAPB, and polymer **MTI-COF-1**. (B) FTIR spectra of monomers MTA and TAPA, and polymer **MTI-COF-2**. (C,D) Experimental (red line for **MTI-COF-1**; blue for **MTI-COF-2**) versus Pawley refined (black line) versus their corresponding simulated (dark green for AA; light green for AB stacking) PXRD data. The refinement agreements for **MTI-COF-1** are R_{wp} = 3.77% and R_p = 2.93%, and for **MTI-COF-2** R_{wp} = 3.71% and R_p = 2.83%. [Color figure can be viewed at wileyonlinelibrary.com]

temperatures are lower than reported decomposition temperatures of polyimide COFs (>400 °C).[8,12,13] This observation may be an indication of an amount of polyamic acid intermediate to be still present in the frameworks (possibly explaining the first decomposition step in Fig. S2), but closer investigation is required. Finally, chemical stability checks in various liquid media were carried out (Supporting Information). Given the synthesis and purification conditions, we conclude that the COFs are stable in organic solvents. While the additional stability checks showed good framework retention in pure water and acid solutions. Alkali aqueous solutions, however, significantly affect the framework stability, as is to be expected for polyimide polymers.[17]

Structural characterization was further carried out by means of powder X-ray diffraction (PXRD) measurements, and the experimental spectra were compared with the computer simulated patterns [Fig. 1(C,D)]. Although both COFs were found to also contain amorphous segments, a well-defined short-range order was observed, which corresponds to theoretically expected micropore sizes: 1.41 nm for **MTI-COF-1** and 1.24 nm for **MTI-COF-2**. In addition, structural optimizations were performed computationally with a classical force field approach (using Materials Studio v8.0, see Supporting Information). During these simulations, both COFs relaxed from a completely flat two-dimensional (2D) sheet to a nonflat configuration, exhibiting torsion within the framework. The main cause was discovered to be a break of 2D symmetry of the triamine linkage molecules TAPB and TAPA. The preferred torsion angles between the outer benzene rings of these segments were calculated to be 33° for **MTI-COF-1** and 36° for **MTI-COF-2**. Similar torsion angles between the MTI segments and the outer benzene rings of TAPB and TAPA were also observed (Supporting Information). Since this transition was self-occurred during the geometry optimization, it indicates that there is no (or small) energy barrier for this transition and that both COFs will naturally obtain a configuration exhibiting torsion. Furthermore, the packing of the 2D polymer sheets was computationally investigated: AA stacking representing adjacent sheets to perfectly overlap and to create straight one-dimensional (1D) channels, and AB stacking representing an offset of one unit cell between neighboring sheets not leading to continuous 1D channel. The most stable conformation in both COFs was the AA stacking mode. The simulated AA stacking PXRD patterns were then utilized as a basis for Pawley refinement of the experimental diffraction patterns. In both cases, a good agreement was obtained [Fig. 1(C,D)], and the crystallographic data of both COFs can be found in the Supporting Information. The simulated PXRD data of the AA stacked COFs matched well with the experimental reflections, and better than for an assumed AB stacking mode.

Scanning electron microscopy (SEM) images of **MTI-COF-1** and **MTI-COF-2** are shown in Figure 2(A,B) and (C,D), respectively. No clear difference in morphology between the two COFs was observed. Both polymers show aggregation of nanosphere particles with sizes of the order of 100–200 nm. In addition, the aggregates reflect the presence of macroporous

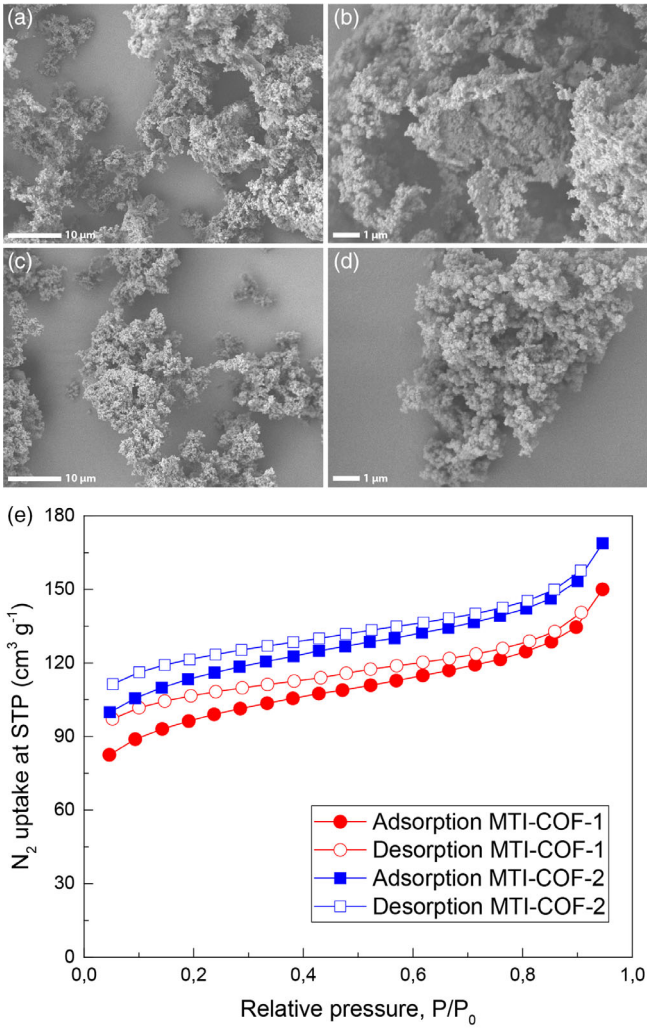

FIGURE 2 (A,B) SEM micrographs of **MTI-COF-1**. (C,D) SEM micrographs of **MTI-COF-2**. (E) Nitrogen sorption isotherms of **MTI-COF-1** (red) and **MTI-COF-2** (blue) measured at 77 K. [Color figure can be viewed at wileyonlinelibrary.com]

structures. To quantify the porosity levels more quantitatively, nitrogen gas sorption measurements were performed [Fig. 2 (E)]. The isotherms of both COFs resemble typical Type II isotherms, which confirm the presence of micropores. The surface areas of both COF samples were calculated through the Brunauer–Emmett–Teller (BET) theory. Both COFs exhibited a good porosity level, with BET surface areas of 339 $m^2\ g^{-1}$ for **MTI-COF-1** and 397 $m^2\ g^{-1}$ for **MTI-COF-2**. Such values are within the range of surface areas of state-of-the-art microporous polymers, and it is expected that further improvement of the polymerization conditions could contribute to an even more porous structure. Additionally, pore size distributions were calculated on the basis of the nitrogen isotherms (Fig. S2). Although it was not possible to extract specific micropore sizes from these isotherms, the pore size distributions were centered around the lower limit of mesopores (2 nm) and expectedly more so around the micropores.

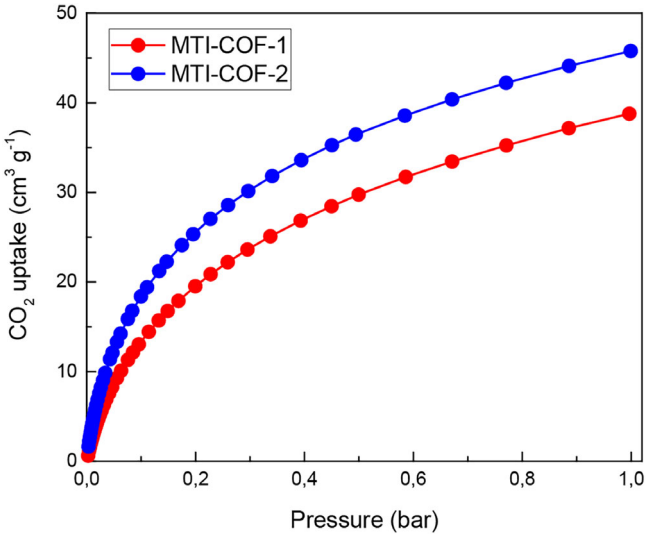

FIGURE 3 Carbon dioxide adsorption isotherms of **MTI-COF-1** (red) and **MTI-COF-2** (blue) measured at 273 K. [Color figure can be viewed at wileyonlinelibrary.com]

Additionally, the CO_2 adsorption performance of **MTI-COF-1** and **MTI-COF-2** was determined. The isotherms were measured at 273 K over a range of 3–997 mbar, and the data are shown in Figure 3, using the conventional protocol of plotting CO_2 uptake versus the absolute pressure. CO_2 capacities at 273 K and 1 bar were measured to be 39 and 46 $cm^3\ g^{-1}$ for **MTI-COF-1** and **MTI-COF-2**, respectively. Interestingly, despite having different molecular sizes and physicochemical adsorption mechanisms, both nitrogen and carbon dioxide gas adsorbed better to **MTI-COF-2** than to **MTI-COF-1**. A possible reason for this is the large difference of the *c* lattice parameter between the two porous polymers (as a result of the difference in torsion angles reported earlier), which is 3.7 Å for **MTI-COF-1**, and 4.2 Å for **MTI-COF-2**. A larger *c* lattice parameter could cause elongation of the 1D COF channels, which exposes a larger accessible area for gas molecules. At the same time, it is likely that such a large interlayer distance allows gas to not only enter the COF via the 1D channel ends, but parallel to the layers as well.

Nevertheless, the CO_2 storage capacity values for both polymers are relatively high, considering the fact that no additional pore surface engineering was used to further enhance the capacities.[18] Incorporation of CO_2 fixating groups along the polymer backbone,[19,20] might also be a strategy applicable to COF research in order to increase the CO_2 storage capacity values even further. In addition, these MTI-based porous polymers are among the first polyimide polymers to be employed as CO_2 gas hosts, and their CO_2 uptake is already comparable to that of the widely tested imine, triazine, and boronate ester COFs.[21] Also, a pressing issue of competing metal–organic frameworks, and boronate ester COFs is their lack of good performance in CO_2 uptake under humid conditions or in general their hydrolytic stability.[22–24] The porous materials presented in this research, however, are expected to not be affected by humidity because of the general stability of polyimides in aqueous environments. Research to confirm this expectation has been initiated and the results will be reported elsewhere.

In summary, MTI COFs have been synthesized in high yields through imidization of MTA with two different triamines. Both COFs displayed short-ranged crystalline order, corresponding to expected micropore sizes. Computational studies revealed that the 2D polymer sheets were adopting a nonflat configuration, due to torsions between the linking monomers. Both COFs exhibited porous structures with good surface areas, and affinities toward nitrogen and carbon dioxide gasses. The combination of high surface areas with micropores makes these porous polymers good candidates for separation fields, as well as energy storage applications, considering their expected redox activities.

EXPERIMENTAL

Synthesis of MTI-COFs

A 10 mL Pyrex tube was charged with MTA (144.1 mg, 0.5 mmol), and TAPB (175.7 mg, 0.5 mmol) or TAPA (145.2 mg, 0.5 mmol) in a solution of *m*-cresol/*N*-methylpyrrolidone (4 mL/4 mL). The reaction mixture was stirred for 5 min and sonicated for 2 min. Isoquinoline (0.1 mL) was added, after which the tube was directly degassed via three freeze–pump–thaw cycles at 77 K, and subsequently flame sealed. Then, the tube was heated in an oven at 150 °C for 3 days. The resulting precipitate was washed with methanol (3 × 10 mL) and acetone (3 × 10 mL) and recovered by centrifugation. The resulting compound was purified by Soxhlet extraction in THF for 16 h, and then dried at 60 °C under vacuum for 16 h to provide **MTI-COF-1** as an ochre powder (275 mg, 94%) and **MTI-COF-2** as a brown powder (239 mg, 91%).

MTI-COF-1: Infrared (IR) [attenuated total reflection (ATR)]: ν = 1778 (w), 1727 (s), 1669 (m), 1605 (m), 1514 (s), 1372 (bs), 1125 (m), 816 (s) cm^{-1}.

MTI-COF-2: IR (ATR): ν = 1778 (w), 1725 (s), 1666 (m), 1606 (m), 1505 (s), 1381 (bm), 1319 (bm), 1275 (bm), 1125 (m), 819 (bm) cm^{-1}.

See Supporting Information for synthesis of MTA, characterization details, and crystallographic data.

ACKNOWLEDGMENTS

A. Nagai dedicates this manuscript to Prof Takeshi Endo in recognition of his inspirational mentorship and groundbreaking achievements in the field of polymer chemistry. The authors also thank Dalian University of Technology for the permission to use their Materials Studio software package.

REFERENCES AND NOTES

1 X. Feng, X. Ding, D. Jiang, *Chem. Soc. Rev.* **2012**, *41*, 6010.

2 S. S. Han, H. Furukawa, O. M. Yaghi, W. A. Goddard, *J. Am. Chem. Soc.* **2008**, *130*, 11580.

3 H. Fan, J. Gu, H. Meng, A. Knebel, J. Caro, *Angew. Chem. Int. Ed.* **2018**, *57*, 4083.

4 C. R. DeBlase, K. E. Silberstein, T.-T. Truong, H. D. Abruña, W. R. Dichtel, *J. Am. Chem. Soc.* **2013**, *135*, 16821.

5 S. B. Alahakoon, C. M. Thompson, G. Occhialini, R. A. Smaldone, *ChemSusChem* **2017**, *10*, 2116.

6 A. P. Côté, A. I. Benin, N. W. Ockwig, M. O'Keeffe, A. J. Matzger, O. M. Yaghi, *Science* **2005**, *310*, 1166 LP.

7 H. M. El-Kaderi, J. R. Hunt, J. L. Mendoza-Cortés, A. P. Côté, R. E. Taylor, M. O'Keeffe, O. M. Yaghi, *Science* **2007**, *316*, 268 LP.

8 Q. Fang, Z. Zhuang, S. Gu, R. B. Kaspar, J. Zheng, J. Wang, S. Qiu, Y. Yan, *Nat. Commun.* **2014**, *5*, 1.

9 F. J. Uribe-Romo, C. J. Doonan, H. Furukawa, K. Oisaki, O. M. Yaghi, *J. Am. Chem. Soc.* **2011**, *133*, 11478.

10 C. R. DeBlase, W. R. Dichtel, *Macromolecules* **2016**, *49*, 5297.

11 S. Kandambeth, D. B. Shinde, M. K. Panda, B. Lukose, T. Heine, R. Banerjee, *Angew. Chem. Int. Ed.* **2013**, *52*, 13052.

12 Q. Fang, J. Wang, S. Gu, R. B. Kaspar, Z. Zhuang, J. Zheng, H. Guo, S. Qiu, Y. Yan, *J. Am. Chem. Soc.* **2015**, *137*, 8352.

13 L. Jiang, Y. Tian, T. Sun, Y. Zhu, H. Ren, X. Zou, Y. Ma, K. R. Meihaus, J. R. Long, G. Zhu, *J. Am. Chem. Soc.* **2018**, *140*, 15724.

14 K. A. McMenimen, D. G. Hamilton, *J. Am. Chem. Soc.* **2001**, *123*, 6453.

15 J. B. Carroll, M. Gray, K. A. McMenimen, D. G. Hamilton, V. M. Rotello, *Org. Lett.* **2003**, *5*, 3177.

16 Y. Kofuji, S. Ohkita, Y. Shiraishi, H. Sakamoto, S. Ichikawa, S. Tanaka, T. Hirai, *ACS Sustain. Chem. Eng.* **2017**, *5*, 6478.

17 L. E. Stephans, A. Myles, R. R. Thomas, *Langmuir* **2000**, *16*, 4706.

18 N. Huang, R. Krishna, D. Jiang, *J. Am. Chem. Soc.* **2015**, *137*, 7079.

19 B. Ochiai, K. Yokota, A. Fujii, D. Nagai, T. Endo, *Macromolecules* **2008**, *41*, 1229.

20 M. Sakuragi, N. Aoyagi, Y. Furusho, T. Endo, *J. Polym. Sci. Part A: Polym. Chem.* **2014**, *52*, 2025.

21 Y. Zeng, R. Zou, Y. Zhao, *Adv. Mater.* **2016**, *28*, 2855.

22 A. C. Kizzie, A. G. Wong-Foy, A. J. Matzger, *Langmuir* **2011**, *27*, 6368.

23 J. Liu, J. Tian, P. K. Thallapally, B. P. McGrail, *J. Phys. Chem. C* **2012**, *116*, 9575.

24 L. M. Lanni, R. W. Tilford, M. Bharathy, J. J. Lavigne, *J. Am. Chem. Soc.* **2011**, *133*, 13975.